

A MACHINE-LEARNING METHOD FOR TIME-DEPENDENT WAVE EQUATIONS OVER UNBOUNDED DOMAINS

CHANGJIAN XIE, JINGRUN CHEN, AND XIANTAO LI

ABSTRACT. Time-dependent wave equations represent an important class of partial differential equations (PDE) for describing wave propagation phenomena, which are often formulated over unbounded domains. Given a compactly supported initial condition, classical numerical methods reduce such problems to bounded domains using artificial boundary condition (ABC). In this work, we present a machine-learning method to solve this type of equations as an alternative to ABCs. Specifically, the mapping from the initial conditions to the PDE solution is represented by a neural network, trained using wave packets that are parameterized by their band width and wave numbers. The accuracy is tested for both the second-order wave equation and the Schrödinger equation, including the nonlinear Schrödinger equation. We examine the accuracy from both *interpolations* and *extrapolations*. For initial conditions lying in the training set, the learned map has good interpolation accuracy, due to the approximation property of deep neural networks. The learned map also exhibits some good extrapolation accuracy. We also demonstrate the effectiveness of the method for problems in irregular domains. Overall, the proposed method provides an interesting alternative for finite-time simulation of wave propagation.

1. INTRODUCTION

Wave propagation is an ubiquitous phenomenon and for a long time, the associated properties have been a subject of interest in many disciplines [49]. Aside from the well known acoustic waves, the Schrödinger equation that describes electronic waves, and the elastodynamics that embodies stress waves [21] are also important examples. These models share the common ground that waves often propagate in an unbounded domain, even though they are triggered locally, e.g., by the presence of a wave source or an external forcing.

One classical numerical approach to treat wave propagation in an unbounded domain is the absorbing boundary condition (ABC), which confines the computation to a finite domain, and an ABC is then imposed on the boundary to minimize undesirable reflections [3, 9, 20, 24, 27]. Rather than simply removing the exterior region, the ABC provides an efficient approach to mimic the influence from the surrounding environment. There are several different approaches to construct and implement ABCs, most of which involve the derivation and approximation of the Dirichlet-to-Neumann map. There has been a large body of works on ABCs and interested readers may refer to the review articles [1, 24] for details and references therein. The integration of ABCs with finite difference or finite element methods, has also been extensively studied [38, 41, 46].

Recently, the rapid progress in deep learning has driven the development of solution techniques for PDEs under the framework of deep learning, especially in high-dimensional cases where deep neural networks (DNNs) are expected to overcome the curse of dimensionality; see [16] for a review and [7, 8, 11, 17, 19, 28, 31, 35, 37, 40, 43, 47, 57] for specific examples. One remarkable application of neural networks is the physics-informed neural networks (PINNs) [43], which has demonstrated its accuracy in solving both forward problems and inverse problems, where model parameters are inferred from the observed data. PINNs have already been applied to a range of problems, including those in fluid dynamics [33, 44], meta-material design [13], biomedical engineering [55], uncertainty quantification [52]

Date: July 21, 2021.

2010 Mathematics Subject Classification. 65M99, 68T20, 68W25.

Key words and phrases. Machine learning, wave equation, unbounded domain.

and free boundary problems, besides the high dimensional PDEs and stochastic differential equations. Typically, the loss function is defined over a *finite* domain in most methods, such as the deep Ritz method [19], deep Galerkin method [47], physics-informed neural networks [43], and deep mixed residual method [40]. To the best of our knowledge, the only exceptions are the full history recursive multilevel Picard approximation method [7, 31] and the deep backward stochastic differential equation method [17, 28], where the solution of the underlying PDE is approximated through the solution of a suitable stochastic optimization problem on an appropriate function space. Typical equations are (semilinear) parabolic PDEs. These recent works have demonstrated the strong representability of DNNs for solving PDEs.

The current work aims to solve time-dependent wave equations on *unbounded* domains using deep learning. One natural approach is to build an artificial neural network (ANN) that takes an ABC, e.g., the perfectly matched layer (PML) method, into account [53, 54]. The basic idea behind the approach in [53] is as follows. Given the electromagnetic field at the current step, one can predict the field on the PML boundary at next time step. Then, one computes a field in a slightly larger domain, called the object domain, at the next step through output from PML, which subsequently becomes the new input data, by the finite-difference time-domain (FDTD) method. Furthermore, one can embed the network model into the FDTD method and replace the PML. The data groups are collected at the interface with conventional PML. The Long Short Term Memory (LSTM) network based on the PML model in [54] can achieve higher accuracy than an ANN that is based on the PML model, thanks to the sequence dependence feature of LSTM networks. Compared to the conventional PML approach, the machine-learning methods in [53, 54] decrease the size of the boundary region and the complexity of the FDTD method, due to the introduction of a one-cell boundary layer. But the data generation involves prior PML computation. This process involves the history of solutions at the boundary and may be rather complicated in general. We propose a different machine-learning strategy to solve the wave propagation over unbounded domain. Given a compactly supported initial condition, we restrict the full problem to a solution mapping over a finite region. More specifically, the mapping from the initial condition, expressed as wave packets with band width and wave numbers as parameters, to the PDE solution in the same compactly supported domain at later times, is represented by a fully connected neural network or residual neural network. The parameters in the network are then trained using data that can be generated using a variety of methods, ranging from analytical solutions, numerically computed solutions, to approximated solution from PINNs.

On one hand, the mapping can generate accurate results in which the specific initial condition is not included in the training set, but can be interpolated by those in the training set. On the other hand, the method also allows extrapolations, e.g., when the wave packet arrives at the boundary of the finite region, even though the training set only contains temporal instances prior to that event. Compared to existing works, the proposed method can be easily implemented. The solutions represented by DNN also exhibit absorbing properties. But there is no need to determine the coefficients in ABCs, or to incorporate ABCs into finite difference or finite element methods. The proposed method provides an alternative for finite-time simulation of wave propagation.

This paper is organized as follows. In section 2, we describe the machine-learning method for two representative wave equations: the second-order wave equation and the Schrödinger equation. Numerous examples are provided to show the interpolative and extrapolative properties of the proposed method in section 3. Conclusions are drawn in section 4.

2. METHODOLOGY

To elaborate the approach of constructing solution representations by a neural network, we consider, as specific examples, the time-dependent acoustic wave equation and the Schrödinger equation as examples, due to the fact that they have been treated extensively in PDE analysis and numerical approximations. But we expect that the idea can be extended to other types of wave equations. We express these two models as time-dependent PDEs over the entire space \mathbb{R}^d :

(I) Time-dependent wave equation:

$$(2.1) \quad \begin{aligned} u_{tt} &= \Delta u, \quad \mathbf{x} \in \mathbb{R}^d, \quad t > 0, \\ u(\mathbf{x}, 0) &= u_0(\mathbf{x}), \quad u_t(\mathbf{x}, 0) = v_0(\mathbf{x}). \end{aligned}$$

(II) Time-dependent Schrödinger equation:

$$(2.2) \quad \begin{aligned} i\partial_t u(\mathbf{x}, t) &= -\Delta u(\mathbf{x}, t) + V(\mathbf{x}, t)u(\mathbf{x}, t) + f(|u(\mathbf{x}, t)|^2)u(\mathbf{x}, t), \quad \mathbf{x} \in \mathbb{R}^d, \quad t > 0, \\ u(\mathbf{x}, 0) &= u_0(\mathbf{x}), \quad \mathbf{x} \in \mathbb{R}^d. \end{aligned}$$

There are important cases that deserve particular attention:

- (a) The linear Schrödinger equation: $f \equiv 0$. This describes the dynamics of a free electron.
- (b) The cubic Schrödinger equation:

$$(2.3) \quad f(\rho) = \beta\rho, \quad \rho \in [0, \infty),$$

where β (positive for repulsive or defocusing interaction and negative for attractive or focusing interaction) is a given dimensionless constant describing the strength of the interaction. It has been widely used to model nonlinear wave interactions in a dispersive medium.

We have expressed these models in their non-dimensionalized forms. For example, the wave speed in (2.1) and the Planck constant in (2.2) have been both set to unity. In addition, we set $\beta = -1$ in (2.3).

We make the important assumption that the initial condition and the potential are compactly supported in a finite domain, denoted by $\Omega \subset \mathbb{R}^d$, that is,

$$\text{supp}(u_0), \text{supp}(v_0), \text{supp}(V) \subset \Omega.$$

Our aim is to determine the solution $u(\cdot, t)$ in the same domain Ω at later times.

2.1. The training procedure. In this section, we describe how the solution is trained using neural networks. One key step in a machine learning procedure is the preparation of a dataset, which will subsequently be fed into the machine learning model. We first prepare a dataset, consisting of the initial condition and the corresponding solutions at later times. We will denote initial data by $U_0 = (u_0, \partial_t u_0)$ for time-dependent wave equation (2.1) and $U_0 = (p_0, q_0)$ for the time-dependent Schrödinger equation (2.2) with p and q being the real and imaginary parts of the wave function, respectively. In principle, the mapping from U_0 to the solution at a later time can be expressed as an operator \mathcal{S} ,

$$(2.4) \quad u(\mathbf{x}, t)|_{\Omega} = \mathcal{S}U_0.$$

For example, in the linear case, this can be written as an integral operator using the Green's function [22]. But such an expression is of limited value in practice since the direct evaluation is rather expensive. Here we represent such a mapping using a neural network and determine the parameters through training.

In the training step, we consider three cases, as motivated by the terminology in control systems,

(I) Single-input single-output (SISO) datasets

$$(2.5) \quad \left\{ U_0^\ell, U_T^\ell \right\}_{\ell=1}^N.$$

(II) Single-input multiple-output (SIMO) datasets

$$(2.6) \quad \left\{ U_0^\ell, U_{\{t_i\}_{i=1}^p}^\ell \right\}_{\ell=1}^N$$

(III) Exogenous-input multiple-output (XIMO) datasets

$$(2.7) \quad \left\{ V_{\{t_i\}_{i=1}^p}^\ell, U_{\{t_i\}_{i=1}^p}^\ell \right\}_{\ell=1}^N.$$

Here the integer N denotes the number of training samples, and p refers to the time instances where the solutions are observed. The *input* simply refers to the initial conditions and the output involves the resulting solutions at a later time (or at multiple time instances). Namely, $U_T := \{u(\cdot, T)\}$. These solutions will be collected at grid points that lie in the domain of interest Ω . For simplicity, we also work with U_T^ℓ in the same domain. But in practice, one can also choose U_T in a different domain. In the case of XIMO, one may consider the Schrödinger equation, with the initial condition fixed at ground state. The dynamics is then entirely driven by the external potential.

We will discuss the construction of datasets in the next section in more details. In particular, properties of wave propagations, e.g., wave length and dispersion relations, are built into the training set. Our experience suggests that properly rescaling the input data can improve the convergence. Specifically, before it is fed into the network, the initial condition will go through the following transformation.

$$U_0 \rightarrow \frac{2(\lambda U_0 - \inf(U_0))}{\sup(U_0) - \inf(U_0)} - \inf(U_0),$$

where $\inf(U_0)$ and $\sup(U_0)$ denote the infimum and supremum of U_0 , respectively. Note that after the rescaling, the input data U_0 take values in $[-1, 1]$. Since U_T is fully determined by U_0 , we approximate the mappings from U_0 to U_T using a neural network, denoted by $\mathcal{N}_D^M(U_0, \mathcal{W})$, i.e.,

$$(2.8) \quad U_T \approx \mathcal{N}_D^M(U_0, \mathcal{W}).$$

The neural network underlying the mapping (2.8) is illustrated in Figure 1.

The function \mathcal{N}_D^M is determined by a network consisting of D layers with width M , and the associated parameters are denoted by \mathcal{W} . For a fully connected neural network (FCNN), the mapping (2.8) from input to output is explicitly given by

$$(2.9) \quad \mathcal{N}_D^M(U_0, \mathcal{W}) = W_D^T \mathcal{H}_{D-1}^M(U_0, \tilde{\mathcal{W}}) + b_D,$$

where,

$$\mathcal{H}_{D-1}^M(U_0, \tilde{\mathcal{W}}) = \phi(W_{D-1}^T \cdots \phi(W_2^T \phi(W_1^T U_0 + b_1) + b_2) \cdots + b_{D-1}),$$

with ϕ being the activation function and $\{W_j, b_j\}_{j=1}^D$ being the parameters specified by the network.

The residual neural network (ResNet) structure [29] will also be considered in our numerical studies. In this case, the mapping can be expressed with the following steps,

$$\begin{cases} y_1 = W_1^T U_0 + b_1, \\ y_2 = y_1 + \mathcal{H}_{D_1}^M(y_1), \\ y_3 = y_2 + \mathcal{H}_{D_2}^M(y_2), \\ \cdots \quad \cdots \quad \cdots \\ y = y_s + \mathcal{H}_{D_s}^M(y_s), \\ \tilde{\mathcal{N}}_D^M(U_0, \mathcal{W}) = W_D^T y + b_D, \end{cases}$$

where s is the number of residual blocks with a skip connection.

The next step is to formulate the problem as a supervised learning problem by means of minimizing the population risk (expected risk), elaborated in [10] by

$$\min_{\mathcal{W}} \mathbb{E}_{(u_0, u_T) \sim \mu} [\|\mathcal{N}_D^M(u_0, \mathcal{W}) - u_T\|^2], \text{ or } \min_{\mathcal{W}} \mathbb{E}_t \mathbb{E}_{(u_0, u(t)) \sim \mu} [\|\mathcal{N}_D^M(u_0, \mathcal{W}) - u(t)\|^2],$$

with μ being a probability distribution, which in practice, can be discretized by mean squared error as empirical loss for the training samples. For example, for a SISO dataset, this leads to a cost function,

$$(2.10) \quad \mathcal{L}(U_0, \mathcal{W}) = \frac{1}{N} \sum_{\ell=1}^N [\mathcal{N}_D^M(U_0^\ell, \mathcal{W}) - u_T^\ell]^2.$$

Similarly, for a SIMO dataset, we can define the loss function as follows,

$$(2.11) \quad \mathcal{L}(U_0, \mathcal{W}) = \frac{1}{N} \sum_{i=1}^p \sum_{\ell=1}^N \left[\mathcal{N}_D^M(U_0^\ell, \mathcal{W}) - u_{\{t_i\}_{i=1}^p}^\ell \right]^2.$$

Notations for the parameters of our model and algorithm are summarized in Table 1.

d	the dimension of the problem
\mathcal{K}	the set of wave numbers of wave packet
Σ	the set of width of wave packet
D	number of layers
M	number of neurons of each hidden layer
N	number of initial conditions (training samples)
m_1	number of column of input matrix
m_2	number of column of output matrix
p	number of time instances
$(\cdot)_F = \mathcal{N}_D^M$	representation of fully connected neural networks
$(\cdot)_R = \tilde{\mathcal{N}}_D^M$	representation of residual neural networks
β	constant describing the strength of interaction
λ	rescaling parameter of input data
s	number of residual blocks
E	exponential spacing with $\Sigma = \{h, 2h, 2^2h, 2^3h, 2^4h, 2^5h\}$
L	linear spacing with $\Sigma = \{0.8, 0.9, 1, 1.1, 1.2, 1.3\}$
δt	time step
p	the real part of wave function
q	the imaginary part of wave function
\mathcal{R}	the L^2 relative error between the reference and DNN solution

TABLE 1. Notations for the parameters in the model (2.9) and algorithm.

In addition to the structure of the network, another factor that may play a significant role in the approximation (2.8) is the choice of the activation function. In this paper, we first pick the FCNNs with the widely used *relu* activation function. Then we implement a number of other nonlinear activation functions to test their accuracy, including:

$$\begin{aligned} \text{relu}(x) = x_+ &= \begin{cases} x, & x > 0, \\ 0, & \text{otherwise,} \end{cases} & \tanh(x) &= \frac{\exp(x) - \exp(-x)}{\exp(x) + \exp(-x)} \\ \text{sigmoid}(x) &= \frac{1}{1 + \exp(-x)}, & \text{elu}(x) &= \begin{cases} x, & x > 0, \\ \alpha(\exp(x) - 1), & \text{otherwise.} \end{cases} \end{aligned}$$

Our remaining task is to **(i)** collect a suitable set of initial conditions and the corresponding solutions at later times, so that the representation (2.8) can be trained; **(ii)** test the approximation (2.8) against analytical or numerical solutions.

2.2. The training set for time-dependent wave equation. Typical analysis of wave propagations starts with their dispersion properties using Fourier transform [49]. For the time-dependent wave equation (2.1), the dispersion relation is given by $\omega(\mathbf{k}) = |\mathbf{k}|$ with \mathbf{k} being the wave number. Often observed in practice are wave packets that are confined by an envelop and travel as a unit. Here we use wave packets to form the training set. More specifically, we consider those wave packets with a

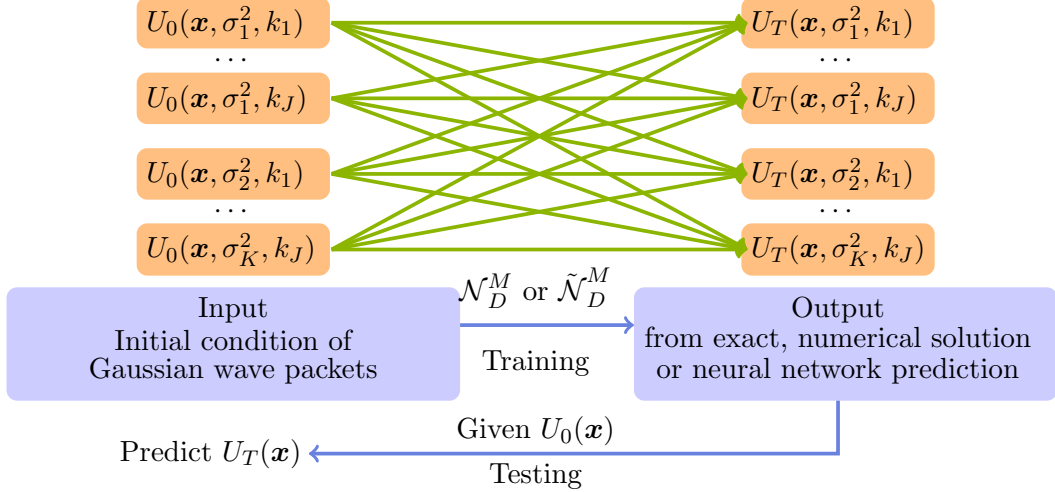


FIGURE 1. Schematic of learning mapping \mathcal{N}_D^M (FCNNs) or $\tilde{\mathcal{N}}_D^M$ (ResNets) from initial condition of Gaussian wave packets with compact support to the output data from exact, or numerical solution, or neural network prediction for the time-dependent wave equations.

Gaussian envelop, which can be derived, e.g., by using Fourier transform. For instance, for the acoustic wave equation (2.1), from the initial conditions

$$(2.12) \quad u(\mathbf{x}, 0) = \exp\left(-\frac{|\mathbf{x}|^2}{2\sigma^2}\right) \cos(\mathbf{k} \cdot \mathbf{x}), \quad \mathbf{x} \in \mathbb{R}^d, \quad \mathbf{k} \in \mathcal{K}, \quad \sigma^2 \in \Sigma,$$

one obtains,

$$(2.13) \quad u(\mathbf{x}, t) = \exp\left(-\frac{\sum_{i=1}^d (x_i - t)^2}{2\sigma^2}\right) \cos(\mathbf{k} \cdot \mathbf{x} - |\mathbf{k}|t), \quad \mathbf{x} \in \mathbb{R}^d.$$

This implies that the initial velocity is given by,

$$(2.14) \quad u_t(\mathbf{x}, 0) = \exp\left(-\frac{|\mathbf{x}|^2}{2\sigma^2}\right) \left[\frac{\sum_{i=1}^d x_i}{\sigma^2} \cos(\mathbf{k} \cdot \mathbf{x}) + |\mathbf{k}| \sin(\mathbf{k} \cdot \mathbf{x}) \right], \quad \mathbf{x} \in \mathbb{R}^d.$$

2.3. The training set for time-dependent Schrödinger equation.

2.3.1. *The linear case.* For the linear Schrödinger equation,

$$(2.15) \quad iu_t = -\Delta u, \quad \mathbf{x} \in \mathbb{R}^d, \quad t > 0,$$

the dispersion relation is given by $\omega(\mathbf{k}) = 1/2|\mathbf{k}|^2$. To form the training set, we first pick the initial conditions from a family of wave packets,

$$(2.16) \quad u_0(\mathbf{x}) = \exp\left[-(\mathbf{x}/\sqrt{2})^2/\sigma^2 + i\mathbf{k} \cdot (\mathbf{x}/\sqrt{2})\right], \quad \mathbf{k} \in \mathcal{K}, \quad \sigma^2 \in \Sigma,$$

representing a Gaussian wave packet centered at the origin with wave number \mathbf{k} . The width parameter of the Gaussian envelope will be drawn from a pre-selected set:

$$\sigma \in \Sigma, \quad \Sigma \subset \Sigma_0(:= \mathbb{R}_+), \quad \mathbf{k} \in \mathcal{K}, \quad \mathcal{K} \subset \mathcal{K}_0(:= \mathbb{R}^d).$$

Theoretically, we can go through the whole spaces \mathcal{K}_0 and Σ_0 . For practical purposes, we take some representative elements from finite subsets \mathcal{K} and Σ . We will discuss more details about the selection of Σ and \mathcal{K} in the next section, and demonstrate how they impact the accuracy.

For each σ and \mathbf{k} , the exact solution to (2.15) can be constructed directly,

$$(2.17) \quad u(x, t) = \frac{1}{\sqrt{1+2it}} \exp\left(-\frac{1}{1+4t^2} \frac{(\frac{x}{\sqrt{2}} - kt)^2}{\sigma^2}\right) \exp\left(i \frac{1}{1+4t^2} [(k + \frac{2tx}{\sqrt{2}}) \frac{x}{\sqrt{2}} - \frac{1}{2}k^2t]\right),$$

for one-dimensional problems ($d = 1$).

For two-dimensional problems ($d = 2$), we have,

$$(2.18) \quad u(x_1, x_2, t) = \left(\frac{i}{i-2t}\right) \exp\left[\frac{-i\left(\frac{x_1^2+x_2^2}{2\sigma^2}\right) - \frac{1}{\sqrt{2}}(k_1x_1 + k_2x_2) + \frac{1}{2}(k_1^2 + k_2^2)t}{i-2t}\right].$$

These formulas can be generalized to arbitrary dimensions d ,

$$(2.19) \quad u(\mathbf{x}, t) = \left(\frac{i}{i-2t}\right)^{\frac{d}{2}} \exp\left[\frac{-i\left(\frac{|\mathbf{x}|^2}{2\sigma^2}\right) - \frac{1}{\sqrt{2}}\mathbf{k} \cdot \mathbf{x} + \frac{1}{2}|\mathbf{k}|^2t}{i-2t}\right].$$

This family of solutions will constitute the datasets defined in (2.5) and (2.6), which will be used in the training step (2.10).

2.3.2. *The nonlinear case.* Since analytical solutions are difficult to obtain for the nonlinear PDE (2.2), we generate the solutions U_T^ℓ using numerical methods. Here we use the finite difference scheme with uniform grid size, together with an operator-splitting scheme in time [5]. More specifically, we use the Strang splitting, which at each time step, involves the following operations:

(a) Solve

$$iu_t + \Delta u = 0,$$

for half of the time step: $\delta t/2$. Due to the linearity, this can be done exactly using the Fourier transform to diagonalize the Laplacian term.

(b) Using the solution from the previous step, solve

$$iu_t + |u|^2u = 0,$$

for one step. Using the fact that $\frac{d}{dt}|u|^2 = 0$, this equation can also be solved exactly. This can also be extended to include an external scalar potential, that is

$$iu_t + (|u|^2 + V(x, t))u = 0,$$

for one step.

(c) Solve $iu_t + \Delta u = 0$ again for another half step.

The symmetric operator splitting is known to have second order accuracy in time. In principle, one can also use higher order methods [56], but the current numerical method is already adequate to test the neural network approximation. We also pick initial conditions from (2.16). The solutions at time T , together with the initial conditions (2.16), will form the data set.

Another interesting approach to build the training set is to design an embedding neural network to obtain the solutions to PDEs; see [19, 40] for examples. We will illustrate this approach using the nonlinear Schrödinger equation as an example. We follow the discrete-time PINNs [43] method, combined with the Crank-Nicolson finite difference scheme (CNFD) [2] in time for (2.2) with $f(\rho) = \beta\rho^\mu$ and $\beta = -1$. Specifically, the discrete-time model is given by

$$(2.20) \quad i \frac{u^{n+1} - u^n}{\delta t} = -\frac{1}{2}\Delta (u^{n+1} + u^n) - \frac{1}{4} [|u^{n+1}|^{2\mu} + |u^n|^{2\mu}] (u^{n+1} + u^n),$$

which can be rewritten, using the representation $u = p + iq$, as follows,

$$\begin{aligned}
(2.21) \quad \mathcal{I}_1(p, q) &= p^{n+1} + \frac{1}{2}\delta t \Delta q^{n+1} + \frac{1}{4}\delta t [(p^2 + q^2)^\mu q]^{n+1} + [(p^2 + q^2)^\mu]^{n+1} q^n \\
&\quad + [(p^2 + q^2)^\mu]^n q^{n+1} - p^n + \frac{1}{2}\delta t \Delta q^n + \frac{1}{4}\delta t [(p^2 + q^2)^\mu q]^n = 0, \\
\mathcal{I}_2(p, q) &= q^{n+1} - \frac{1}{2}\delta t \Delta p^{n+1} - \frac{1}{4}\delta t [(p^2 + q^2)^\mu p]^{n+1} + [(p^2 + q^2)^\mu]^{n+1} p^n \\
&\quad + [(p^2 + q^2)^\mu]^n p^{n+1} - q^n - \frac{1}{2}\delta t \Delta p^n - \frac{1}{4}\delta t [(p^2 + q^2)^\mu p]^n = 0.
\end{aligned}$$

One can parameterize p and q by a neural network and approximate the solution under the total residual loss $\mathcal{I} = \mathcal{I}_1 + \mathcal{I}_2$. In this approach, we consider again those solutions that correspond to the Gaussian wave packets as initial conditions to build the datasets that will be fed into FCNNs and ResNets in high dimensions.

2.4. Optimization. Formulated as an optimization problem, the parameters in the network can be obtained by using the stochastic or batch optimized algorithms, applied to the expected or empirical risks for (2.10) and (2.11). For a comparison of these methods, one can refer to [10]. The prototypical stochastic optimization method is the stochastic gradient descent method in [45], which, in the context of minimizing $\mathcal{L}(U_0, \mathcal{W})$, with \mathcal{W}_0 initialized by [30], is defined by

$$(2.22) \quad \mathcal{W}_{k+1} \leftarrow \mathcal{W}_k - \alpha_k \nabla_{\mathcal{W}_{i_k}} \mathcal{L}(U_0, \mathcal{W}_k),$$

for all $k \in \mathbb{N}$. The index i_k is chosen randomly and α_k is a positive stepsize known as the learning rate. Each epoch of this method is thus very cheap, involving only the computation of the gradient $\nabla_{\mathcal{W}_{i_k}} \mathcal{L}(U_0, \mathcal{W}_k)$ corresponding to one sample. In many cases, a batch approach is a more natural fit. In this paper, we employ the *Adam* method [36] at the beginning of the training process. The convergence will be further improved by using the Broyden-Fletcher-Goldfarb-Shanno (L-BFGS) [42] method.

3. NUMERICAL EXPERIMENTS

In this section, we present numerical examples to test the effectiveness of the neural network representation (2.8). Extensive tests are performed to study the accuracy of the approximation and examine extrapolations by the neural networks. The training samples for the first two examples are based on analytical solutions of the wave equation (2.1), with the first example in 1D and the second example in 3D. We also extend the numerical test to wave equations in 8 dimension where the wave propagation occurs mainly in two dimensions. For the third example, we consider the linear Schrödinger equation (2.2) and build the training set from analytical solutions. In the remaining four examples, we test our method for the cubic Schrödinger equations with solutions computed numerically and the nonlinear Schrödinger equation with data generated from PINNs.

Example 3.1 (The 1D wave equation). Here we first consider the wave equation (2.1) in 1D. The training sets are gathered by (2.5) and (2.6). In the numerical experiments, we take the neural network with $D = 5$ and $m_1 = 2N_x$, $m_2 = N_x$, $M = 100$, both for the FCNNs and ResNets, in the latter case, we choose ResNets with two residual blocks, each block with $D = 2$, $M = 100$ and a skip connection so that the number of parameters of both networks are the same. Meanwhile, we take $N_x = 201$, which is the number of grid points for both the training and testing samples in the spatial domain $[-8, 8]$. The exact training samples are specified by sets \mathcal{K} and Σ . We choose $\mathcal{K} = \{1, 2, \dots, 10\}$. For Σ , we consider two types of selections: a set with linear spacing $L = \{0.8, 0.9, 1, 1.1, 1.2, 1.3\}$, and a set with exponential grid $E = \{h, 2h, 2^2h, 2^3h, 2^4h, 2^5h\}$ where the spacing is doubled each time. We train the networks for 20000 epochs with $\lambda = 1/16$.

After the parameters in the network are determined, the performance of the network approximation is tested on solutions with the following initial conditions,

$$(3.1) \quad u^{\text{I}}(x, 0) = \exp(-x^2) \cos(6x), \quad u_t^{\text{I}}(x, 0) = \exp(-x^2) [2x \cos(6x) + 6 \sin(6x)],$$

$$(3.2) \quad u^{\text{II}}(x, 0) = \exp(-x^2/1.5) \cos(6.5x), \quad u_t^{\text{II}}(x, 0) = \exp(-x^2/1.5) \left[\frac{x}{0.75} \cos(6.5x) + 6.5 \sin(6.5x) \right],$$

$$(3.3) \quad u^{\text{III}}(x, 0) = \operatorname{sech}(x) \cos(2x), \quad u_t^{\text{III}}(x, 0) = \operatorname{sech}(x) [\tanh(x) \cos(2x) + 2 \sin(2x)],$$

$$(3.4) \quad u^{\text{IV}}(x, 0) = \exp(-x^2) \cos(\tilde{k}x), \quad u_t^{\text{IV}}(x, 0) = \exp(-x^2) [2x \cos(\tilde{k}x) + \tilde{k} \sin(\tilde{k}x)],$$

with $\operatorname{sech}(x) = 2/(\exp(x) + \exp(-x))$.

These initial conditions are selected based on the following rationale: We notice that (3.1) is of the same type of initial condition as those in the training sets presented in (2.12) and (2.14). It can be used to verify the training procedure. The initial conditions in (3.2) has a similar function form as those in the training set, but the wave number k and the width σ do not belong to \mathcal{K} and Σ . In view of the selection of \mathcal{K} and Σ , this can be interpreted as an interpolation in terms of the wave number, but an *extrapolation* in terms of the width parameter. The initial condition (3.3) is outside of training sets in the sense that the function form is completely different. For the last initial condition (3.4), the wave number \tilde{k} will be selected as $\tilde{k} = 10.025$ and 10.05 to examine the extrapolation error.

Thanks to the availability of the exact solution, given by the d'Alembert formula, we can quantify the error. Specifically, we define the relative error to be

$$(3.5) \quad \mathcal{R} = \frac{\|u^{\text{DNN}} - u^{\text{REF}}\|_2}{\|u^{\text{REF}}\|_2},$$

where notation u^{REF} denotes the reference solution which can be taken by the exact solution, a numerically computed solution, or an approximated solution from PINNs.

The results, in terms of the relative error of the solutions at time $T = 2$, are shown in Table 2, where we collected the results for the solutions that correspond to the initial conditions (3.1), (3.2) and (3.3), respectively. The results for the first initial condition is hardly surprising, since the initial condition (3.1) is very similar to those in the training set. But our numerical experiments suggest that this method also yields reasonable accuracy for the initial conditions (3.2) and (3.3) that are not the type in the training set. We also observe that in most cases the ResNets yield slightly better accuracy. In this case, using the tanh function with L or $E|_{h=0.5}$ yields the best result. For the third case (3.3), we observe the choice of Σ with linear spacing produces poor results, and it seems important to have a larger range of width parameters in the training set. The results also indicate that the choice of the activation function plays a role. For example, with the choice of the FCNNs and ResNets, the sigmoid function yields slightly worse results, while for the tanh function, the accuracy is much better.

The relative error of solutions at time $T = 2$ from the initial condition (3.4) with various choices of \tilde{k} outside the training set, is shown in Table 3. The training sets are constructed with $\mathcal{K} = \{1, 2, \dots, 10\}$ and $\Sigma = L$. For \tilde{k} from 10.025 to 10.05 the accuracy is reasonable. But we do observe that it deteriorates as \tilde{k} moves further away from \mathcal{K} . Interestingly, for the ResNet with activation functions $\tanh(x)$ and $\operatorname{elu}(x)$, the error grows much more slowly.

Example 3.2 (High dimensional wave equations). In high dimensions, in general, the wave modes are represented by many wave numbers. Here we consider a special case where the variation of the solutions of (2.1) is mainly in the first two dimensions. To this end, we choose training samples specified by $\mathcal{K} = (k_1, k_2, k_3, \dots, k_d)$ with k_1, k_2 both in $\{1, 2, \dots, 5\}$ and $k_i = 1, i = 3, \dots, d$, which indicates that the wave propagation is mostly restricted to they xy -plane. We also choose $\tanh(x)$ and $\Sigma = L$.

Starting with the initial condition (2.12) and (2.14), we use neural network to represent (2.8) with $\mathbf{k} = (2, 2, 1, \dots, 1)$ and $2\sigma^2 = 1$. We take the neural network with $D = 5$, $m_1 = 2N_x N_y$, $m_2 = N_x N_y$ and $M = 100$ of FCNNs. We also take $N_x = N_y = 64$ as the number of grid points for both training

ϕ	Σ	$\mathcal{R}(\times 10^{-3})$		$\mathcal{R}(\times 10^{-3})$		$\mathcal{R}(\times 10^{-2})$	
		u_F	u_R	u_F	u_R	u_F	u_R
relu(x)	$E _{h=0.1}$	3.03	1.36	8.77	2.92	4.92	3.82
	$E _{h=0.5}$	3.15	2.50	7.84	8.13	2.71	2.21
	$E _{h=1}$	3.91	3.60	6.06	14.4	3.09	1.88
	L	2.31	0.985	49.3	33.2	26.7	25.3
tanh(x)	$E _{h=0.1}$	2.31	1.14	2.40	2.05	4.26	3.43
	$E _{h=0.5}$	2.44	1.47	2.10	1.43	0.651	0.373
	$E _{h=1}$	3.61	2.21	2.92	1.81	0.690	0.347
	L	0.797	0.550	4.61	3.53	12.3	11.8
sigmoid(x)	$E _{h=0.1}$	10.4	2.95	2.77	4.12	7.39	3.21
	$E _{h=0.5}$	9.82	3.07	14.9	3.55	5.95	0.642
	$E _{h=1}$	1.32	5.97	26.0	5.69	6.68	0.802
	L	6.41	1.69	29.6	12.5	21.9	13.2
elu(x)	$E _{h=0.1}$	1.60	1.20	3.61	2.47	3.82	3.50
	$E _{h=0.5}$	2.16	1.54	2.97	2.03	1.00	0.443
	$E _{h=1}$	2.79	2.01	2.88	1.91	0.811	0.456
	L	1.05	0.798	6.24	4.26	12.6	12.2

TABLE 2. The approximation error for various choices of activation functions and band width of wave packets for the 1D wave equation (2.1) with FCNNs and ResNets for the initial conditions (3.1) (Left), (3.2) (Middle) and (3.3) (Right). In the training sets, the wave numbers are chosen from $\mathcal{K} = \{1, 2, \dots, 10\}$ and the rescaling parameter $\lambda = 1/16$.

ϕ	\mathcal{K}			\mathcal{K}		
	\tilde{k}	u_F	u_R	\tilde{k}	u_F	u_R
relu(x)	10.025	7.26	5.82	10.05	14.1	11.9
tanh(x)	10.025	1.76	1.54	10.05	1.87	1.64
sigmoid(x)	10.025	6.71	4.13	10.05	12.5	4.36
elu(x)	10.025	1.78	1.73	10.05	2.11	1.88

TABLE 3. Extrapolating the wave number. The approximation of the 1D wave equation with the initial condition (3.4) using different activation functions and band width parameters with FCNNs and ResNets. Choosing $\mathcal{K} = \{1, 2, \dots, 10\}$, $\Sigma = L$ and $\lambda = 1/16$.

and testing in domain $\Omega = [-4, 4] \times [-4, 4]$. We train the networks of 40000 epochs. We increase the dimension from 3D to 8D. The solution at the cross section with the xy -plane at $T = 0.5$ are shown in Figure 2. The relative error are 4.48×10^{-3} (3D) and 1.02×10^{-2} (8D). One can observe that the error grows as the dimension increases.

Example 3.3 (The 1D linear Schrödinger equation). We consider the linear Schrödinger equation (2.15) in the 1D case. The training sets are constructed from (2.16) and (2.17). We consider the

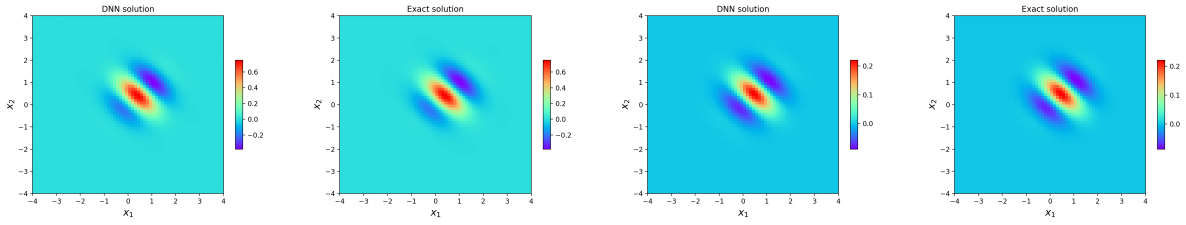


FIGURE 2. Solution of high-dimensional wave equation by DNN (Left) with $\tanh(x)$ up to 40000 iterations, exact solution (Right) evaluated at time $T = 0.5$ to high dimensional wave equation. Left two panel: $d = 3$; Right two panel: $d = 8$.

following initial conditions,

$$(3.6) \quad u_0^{\text{I}}(x) = \exp \left[-\left(\frac{x}{\sqrt{2}}\right)^2 + i3\sqrt{2}x \right],$$

$$(3.7) \quad u_0^{\text{II}}(x) = \exp \left[-\left(\frac{x}{\sqrt{2}}\right)^2/1.2 + i3.25\sqrt{2}x \right],$$

$$(3.8) \quad u_0^{\text{III}}(x) = \exp \left[-\left(\frac{x}{\sqrt{2}}\right)^2 + i\tilde{k}\frac{x}{\sqrt{2}} \right].$$

In the third case, \tilde{k} is to be selected to examine the extrapolation error.

We consider the neural network with $D = 5$, $m_1 = N_x$, $m_2 = N_x$ and $M = 100$ of FCNNs and two residual blocks for ResNets, each block with $D = 2$, $M = 100$. $N_x = 201$ is the number of grid points for both training and testing in the domain $\Omega = [-8, 8]$. The training samples are specified by \mathcal{K} and Σ . We train the networks for 20000 epochs.

We first consider initial conditions (3.6) with $\lambda = 1/4$ and (3.7) with $\lambda = 1/2$ as input, and the corresponding solutions at a single time instance $T = 0.2$ as the output. The results are shown in Table 4. For the initial condition (3.6) the best result is obtained by using the relu function for both FCNN and ResNet. For the initial condition (3.7), the accuracy is not as satisfactory as the previous test, especially when the relu function is used. Another observation is that the result is quite sensitive to the selection of Σ for the training set.

Next we discuss the results from the extrapolation. In this context, an extrapolation can be interpreted in terms of the wave number \tilde{k} in the initial condition (3.8), or in terms of predicting solutions at time instances that are beyond the training period. In the former case, we consider a training set determined by $\mathcal{K} = \{1, 2, \dots, 6\}$, $\Sigma = L$, and $\lambda = 1/2$ and then we pick an initial condition (3.8), where $\tilde{k} \in \{6.025, 6.05\}$. The results are summarized in Table 5. The best result comes from the FCNN with $\text{elu}(x)$. One can see that the error is reasonable for wave numbers in this range, but in all cases the error increases as \tilde{k} moves further away from \mathcal{K} . To visualize the extrapolation in wave number, we take the FCNN with $\text{elu}(x)$ for the best performance which is shown in Figure 3. In the latter case, we consider the solutions with the initial condition (3.6). The training set consists of solutions $(x, t) \in [-8, 8] \times [0, 0.6]$ with $N_x = 201$, $N_t = 11$. Then we test the solution at time T from 0.625 to 0.65, and the results are presented in Table 6. The best result comes from the FCNN using the $\text{elu}(x)$ activation function. But the error grows with T , indicating that the accuracy of the extrapolation can only be guaranteed for a finite time period. To visualize the evolution in time, we take the FCNN with the best performance, together with the activation function $\text{elu}(x)$. The results are shown in Figure 4. A good performance can be guaranteed in short time. But we can see noticeable error for longer times.

Next we test the accuracy of a network trained using a dataset that consists of multiple snapshots of the solutions in the time interval $t \in [0, 3]$ using uniform step size with $N_t = 51$. The network is a FCNN with $D = 5$, $m_1 = N_x$, $m_2 = N_t N_x$ and $M = 100$, activation function $\tanh(x)$, $\mathcal{K} =$

Width	$\mathcal{R}(\times 10^{-3}), \lambda_1$		$\mathcal{R}(\times 10^{-2}), \lambda_2$		Width	$\mathcal{R}(\times 10^{-3}), \lambda_1$		$\mathcal{R}(\times 10^{-2}), \lambda_2$	
	ρ_F	ρ_R	ρ_F	ρ_R		ρ_F	ρ_R	ρ_F	ρ_R
Σ					Σ				
$E _{h=0.1}$	9.19	10.7	4.72	3.86	$E _{h=1}$	2.24	2.24	1.20	4.28
$E _{h=0.5}$	2.38	2.14	2.07	5.62	L	2.96	1.20	2.90	1.81
$E _{h=0.1}$	4.88	9.53	1.17	0.94	$E _{h=1}$	3.02	5.27	0.82	0.54
$E _{h=0.5}$	7.60	8.63	0.63	0.59	L	3.47	3.89	1.93	0.75
$E _{h=0.1}$	10.8	20.6	7.55	1.98	$E _{h=1}$	4.91	7.00	1.08	0.89
$E _{h=0.5}$	11.2	20.9	1.65	1.27	L	3.34	5.09	2.15	1.13
$E _{h=0.1}$	7.02	9.47	1.62	1.00	$E _{h=1}$	2.88	3.05	0.84	0.74
$E _{h=0.5}$	6.22	6.83	0.58	0.69	L	3.36	2.75	1.28	1.01

TABLE 4. Approximation error up to $T = 0.2$ for the 1D linear Schrödinger equation with initial conditions (3.6) and (3.7) using FCNNs and ResNets. From top to bottom: Different choices of activation functions $\text{relu}(x)$, $\text{tanh}(x)$, $\text{sigmoid}(x)$ and $\text{elu}(x)$, and various choices of Σ . The wave numbers are drawn from $\mathcal{K} = \{1, 2, \dots, 10\}$ to build the training set. Taking the scaling parameter $\lambda = \lambda_i$, $i = 1, 2$ with $\lambda_1 = 1/4$, $\lambda_2 = 1/2$.

\mathcal{K}	$\mathcal{R}(\times 10^{-3})$					
	\tilde{k}	p_F	q_F	ρ_F	p_R	q_R
6.025	7.58	8.33	5.43	6.03	6.32	4.04
	6.05	14.3	16.2	11.5	11.4	12.2
6.025	4.78	4.71	3.62	3.93	3.64	3.22
	6.05	7.79	7.64	4.80	6.47	556
6.025	7.65	10.1	6.28	9.17	6.76	9.83
	6.05	13.1	18.8	12.0	11.6	8.82
6.025	3.42	4.03	3.49	3.78	3.92	3.45
	6.05	5.20	6.42	4.71	6.19	6.13

TABLE 5. Extrapolation in the wave number at $T = 0.2$ with FCNNs and ResNets for the initial condition (3.6). From top to bottom: Different choices of the activation functions, $\text{relu}(x)$, $\text{tanh}(x)$, $\text{sigmoid}(x)$ and $\text{elu}(x)$. Choosing $\mathcal{K} = \{1, 2, \dots, 6\}$, $\Sigma = L$ and $\lambda = 1/2$.

$\{1, 2, \dots, 10\}$ and $\Sigma = \{0.8, 0.9, 1, 1.1, 1.2, 1.3\}$. Starting from the initial condition (3.6), Figure 5 shows the prediction by the FCNN, compared to the exact solution. The relative error for the density, the real part, the imaginary part of the wave function are given by 8.900×10^{-3} , 8.025×10^{-3} , 7.606×10^{-3} , respectively. Such examples appear frequently in testing an absorbing boundary condition [3, 32, 50], and the main emphasis is usually on the reflection at the boundary. The results in Figure 5 suggest that the approximation by a FCNN exhibits an absorbing property that is similar to an absorbing boundary condition.

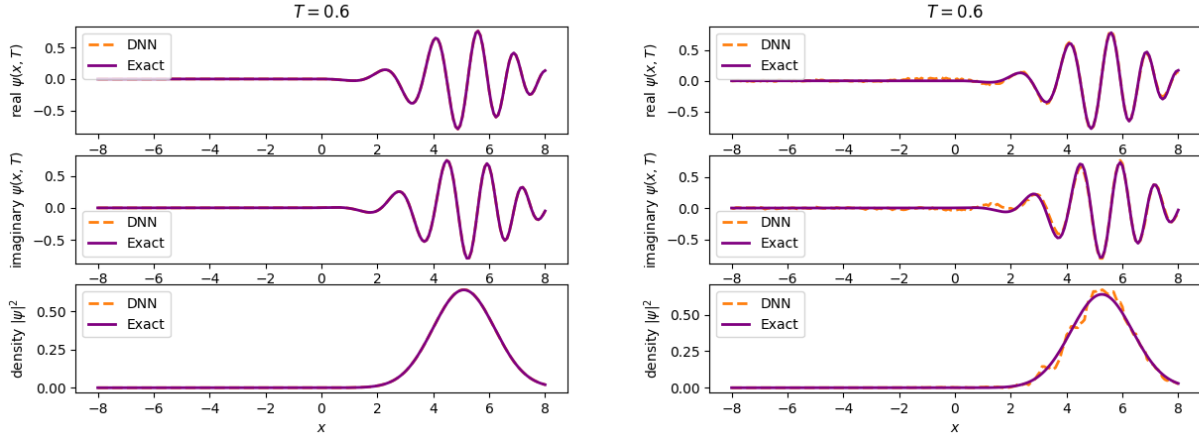


FIGURE 3. Profile of the learned solution at $T = 0.6$ for the 1D linear Schrödinger equation associated with the extrapolation in the wave number by using the activation $\text{elu}(x)$ of FCNNs. Choosing $\mathcal{K} = \{1, 2, \dots, 6\}$, $\Sigma = L$ and $\lambda = 1/2$. Left: $k = 6$; Right: $k = 6.2$.

Later time	$\mathcal{R}(\times 10^{-2})$						
	T	p_F	q_F	ρ_F	p_R	q_R	ρ_R
	0.625	4.69	5.01	4.45	9.45	9.97	8.44
	0.65	7.92	9.68	7.87	18.7	18.4	14.3
	0.625	1.46	1.40	1.31	2.04	2.33	1.56
	0.65	2.95	3.08	2.97	3.36	4.83	2.86
	0.625	1.26	1.74	1.65	2.42	2.68	2.45
	0.65	2.16	2.63	2.85	4.38	5.20	4.43
	0.625	1.31	1.10	1.36	5.12	4.07	3.85
	0.65	2.11	1.94	2.43	11.7	8.19	9.20

TABLE 6. Illustration of extrapolation in time with training sets in $[0, 0.6]$. Different activation functions $\text{relu}(x)$, $\text{tanh}(x)$, $\text{sigmoid}(x)$ and $\text{elu}(x)$ from the top row to the bottom row for the 1D linear Schrödinger equation with the initial condition (3.6) as an input. Choosing $\mathcal{K} = \{1, 2, \dots, 6\}$, $\Sigma = L$ and $\lambda = 1/2$.

Example 3.4 (The 1D cubic Schrödinger equation). Here we test the method on the cubic Schrödinger equation (2.2) in 1D. We use solutions from the following four initial conditions to test the accuracy,

$$(3.9) \quad u_0^{\text{I}}(x) = \begin{cases} -0.5x + 1, & 0 \leq x \leq 2, \\ 0.5x + 1, & -2 \leq x < 0, \\ 0, & \text{otherwise,} \end{cases}$$

$$(3.10) \quad u_0^{\text{II}}(x) = \text{sech}(x) \exp(i5x),$$

$$(3.11) \quad u_0^{\text{III}}(x) = \begin{cases} \exp(-x^2 + i5x), & x \in [-2, 2], \\ 0, & \text{otherwise,} \end{cases}$$

$$(3.12) \quad u_0^{\text{IV}}(x) = \begin{cases} 1 & x \in [-2, 2], \\ 0, & \text{otherwise.} \end{cases}$$

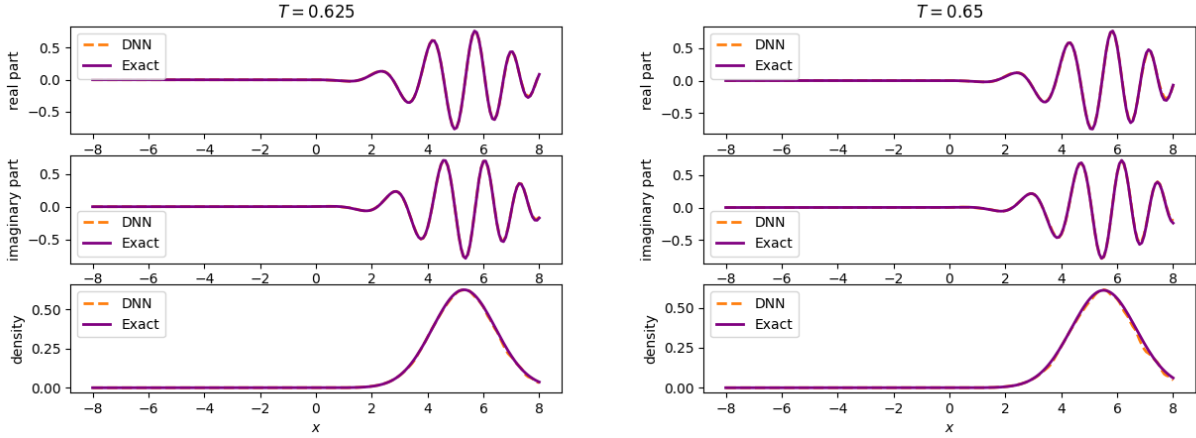


FIGURE 4. Time evolution of the learned solution for the 1D linear Schrödinger equation associated with time extrapolation by using the activation $\text{elu}(x)$ of FCNNs. Choosing $\mathcal{K} = \{1, 2, \dots, 6\}$, $\Sigma = L$ and $\lambda = 1/2$. Left: $T = 0.625$; Right: $T = 0.65$.

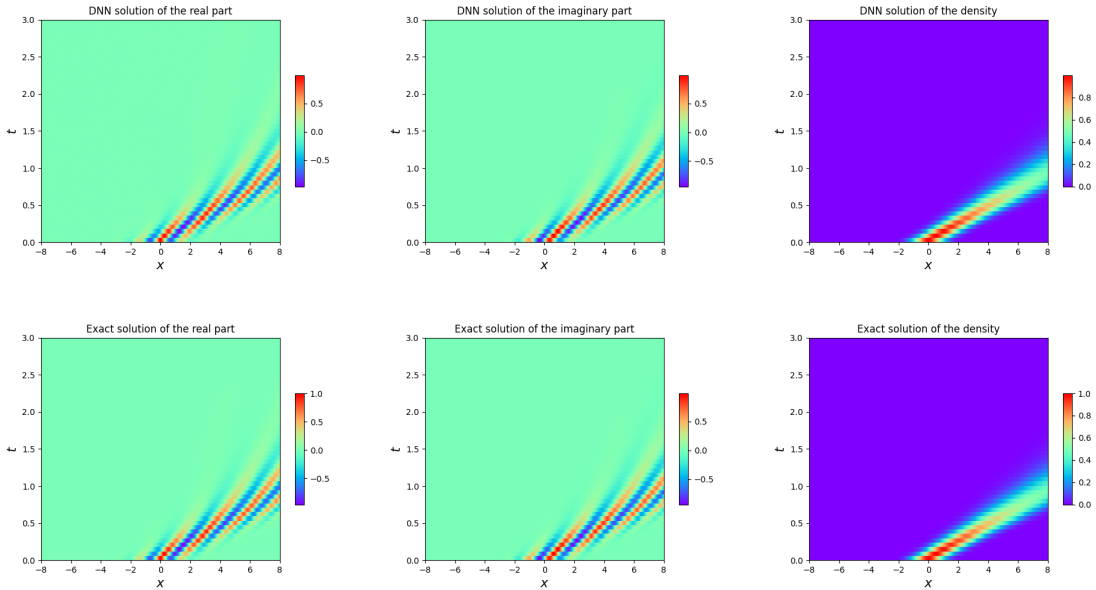


FIGURE 5. A wave packet propagating outside the domain for 1D Schrödinger equation with (3.6) as an input. Top: Prediction by a FCNN with $\tanh(x)$; Bottom: the exact solution. Left: the real part of wave packet solution; Middle: the imaginary part; Right: the electron density ρ .

The first initial condition is the standard hat function. The last initial condition is a square signal with discontinuities at $x = \pm 2$. They have no resemblance with the Gaussian wave packets in the training set.

As demonstrated in the previous section, to generate data, the Strang splitting method, combined with the spectral method [5] are used in the domain $[-\pi\Omega_0, \pi\Omega_0]$ with $\Omega_0 = 16$ and N_x being the

number of Fourier modes. The numerical solution can be captured up to a single-time $T = 1$ with $N_t = 1000$. The training samples are generated by taking $\mathcal{K} = \{1, 2, \dots, 10\}$ and $\Sigma = E$ with $h = 0.5$.

We take FCNNs with $D = 5$, $m_1 = N_x$, $m_2 = N_x$ and $M = 100$, and train the network for 20000 epochs. We pick $N_x = 8192$ both for the training and testing. The results for solutions from initial conditions (3.9) with weak singularity, (3.10) with a smooth profile, (3.11) and (3.12) with discontinuities are presented in Figure 6. The relative errors for the density, the real part and the imaginary part of the wave function are found to be 6.174×10^{-2} , 1.112×10^{-1} , 9.267×10^{-2} for (3.9), and 4.455×10^{-2} , 5.549×10^{-2} , 7.193×10^{-2} , for (3.10), and 1.817×10^{-2} , 2.231×10^{-2} , 2.112×10^{-2} , for (3.11) and 2.325×10^{-1} , 4.339×10^{-1} , 3.923×10^{-1} , for (3.12), respectively, indicating that the smoothness of the solution has an effect on the accuracy of the learned neural network. The last of representations of such solutions in the training set may also be responsible for this outcome.

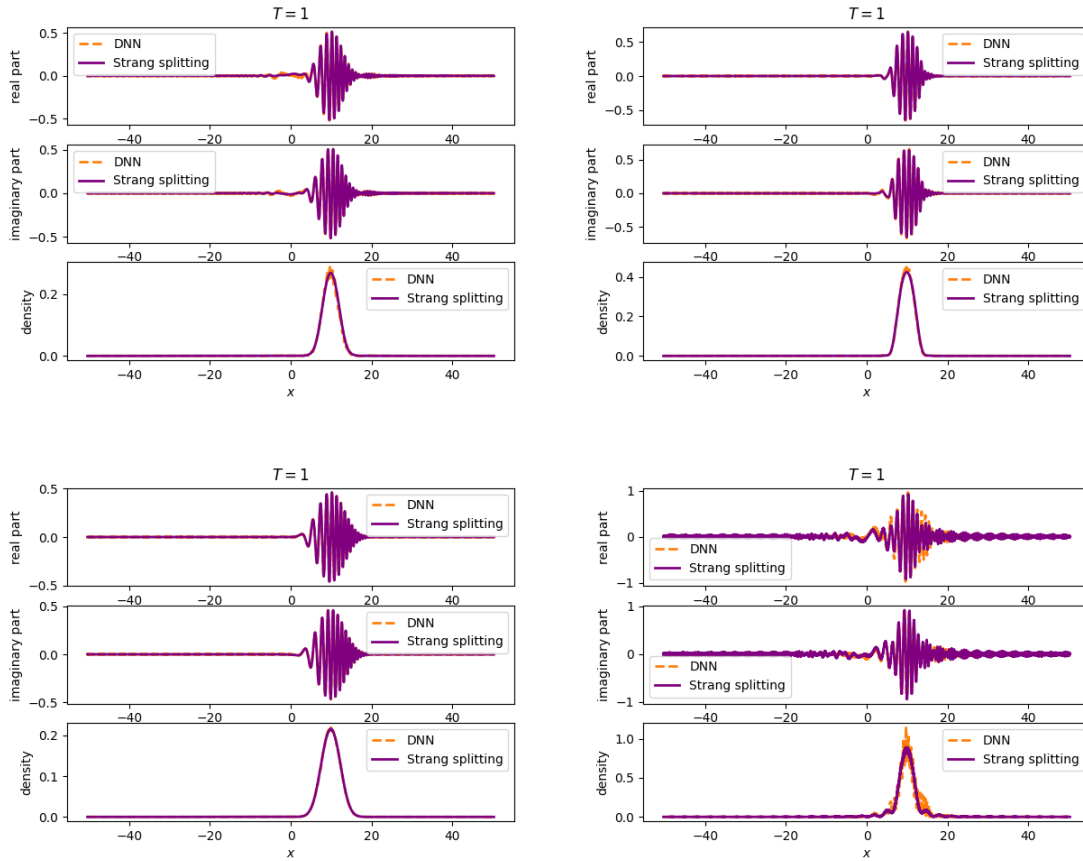


FIGURE 6. The learned solution for the 1D cubic NLS (2.2), the direct numerical solution, and error profile at single-time $T = 1$ with the initial condition (3.9) (top left row) and (3.10) (top right row), (3.11) (bottom left row) and (3.12) (bottom right row). The training samples are created with $\mathcal{K} = \{1, 2, \dots, 10\}$ and $\Sigma = E$ with $h = 0.5$. Here we take tanh as the activation function, and we choose $\lambda = 1$. The network is trained for 20000 iterations. Left panel: the comparison of the solutions; Right panel: the error.

Example 3.5 (1D nonlinear Schrödinger equation with data from a network). In most cases, one can not find the exact solution or numerical solution to train the network. We here consider 1D nonlinear Schrödinger equation and generate data from a network. This would be useful in cases where analytical or standard numerical methods are difficult to implement. As a proof-of-concept example, we use the

PINNs for (2.2) combined with the CNFD (2.20) in time with $f(\rho) = -\rho^\mu$. The real part, imaginary part of wave function can be parameterized by a neural network with total residual loss $\mathcal{I} = \mathcal{I}_1 + \mathcal{I}_2$ in (2.21). The training samples are generated by PINNs with given initial conditions parametrized by $\mathcal{K} = \{1, 2, 3, 4, 5\}$ and various of Σ . We take PINNs with $D = 5$, $m_1 = 1$, $m_2 = 2$ and $M = 100$, and train the PINNs for 10000 epochs. We pick $N_x = 50$ number of points uniformly sampled in $[-\pi\Omega_0, \pi\Omega_0]$ with $\Omega_0 = 1$ both for the training and testing purpose. Once the dataset is ready, we take the FCNNs with $D = 5$, $m_1 = N_x$, $m_2 = N_x$ and $M = 100$ to train the network for 20000 epochs. For the initial condition (3.6), Figure 7 shows the approximation error, for different values of the model parameter μ . An interesting observation, based on the numerical tests for many activation functions and various choices of \mathcal{K} and Σ , is that the nonlinearity has an appreciable impact on the accuracy.

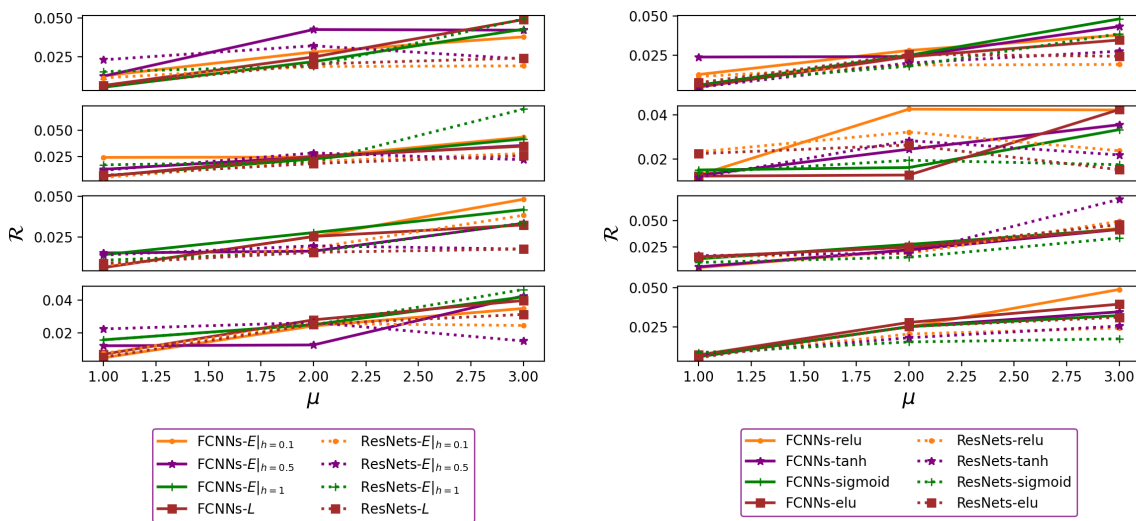


FIGURE 7. Approximation error at $T = 5 \times 10^{-4}$ of the density for the 1D nonlinear Schrödinger equation with initial condition (3.6) using FCNNs and ResNets. Different choices of model parameter $\mu = 1, 2, 3$ and various choices of Σ . The wave numbers are drawn from $\mathcal{K} = \{1, 2, \dots, 5\}$ to build the training set. Here we take $\lambda = 1/4$ and the number of iterations to be 20000. Left (from top to bottom): relu, tanh, sigmoid, elu, as the activation functions; Right (from top to bottom): $E|_{h=0.1}$, $E|_{h=0.5}$, $E|_{h=1}$, L .

Example 3.6 (1D nonlinear Schrödinger equation with a time-dependent potential).

For problems where physical processes are initiated by an external potential, such as Gross–Pitaevskii equation in Bose–Einstein condensate, there are two interesting scenarios: (a) mapping the initial condition to the solution at later time given a potential; (b) mapping the potential to the solution at later time given an initial condition. Motivated by (a), we consider (2.2) given a potential that is compactly supported in space. Absorbing boundary condition for this type of problems can be derived [1].

As a specific example, we consider $V(x, t) = E(t)U(x)$, with time-dependent modulation,

$$(3.13) \quad E(t) = E_0 \exp(-\gamma(t - t_0)^2) \cos(\omega t).$$

The spatial part given by,

$$(3.14) \quad U(x) = \begin{cases} E_0 x(1 - x), & x \in [0, 1], \\ 0, & \text{otherwise,} \end{cases}$$

where E_0 denotes the constant intensity of current. In our test, we take $\gamma = 1$, $E_0 = 1$, $t_0 = 0$ and $\omega = 1$. The network setup is the same as that of example 3.4 except that we use multiple-time output. As comparison, the reference solution is computed numerically using the Strang-splitting method combined with a spectral method with the initial condition (3.10). The training samples are generated with $\mathcal{K} = \{1, 2, \dots, 10\}$ and $\Sigma = E$ with $h = 0.5$. The solution learned by the neural network, along with the solution directly computed are shown in Figure 8. The external potential widens the initial wave packets, which subsequently propagate toward the right boundary. The solution represented by the neural network shows great agreement with the direct solution.

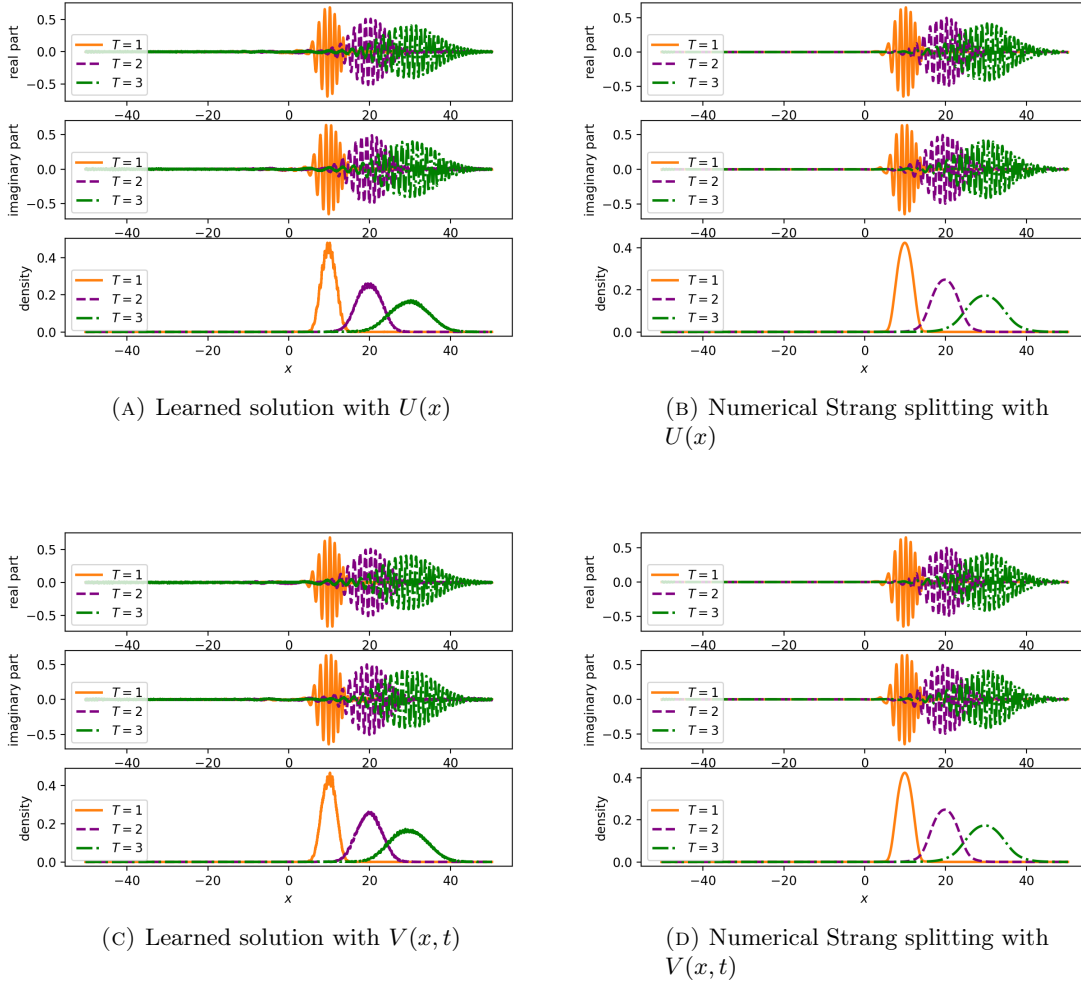


FIGURE 8. The learned solution at multiple-time $T = 1, 2, 3$ for the 1D NLS (2.2) under an external potential function V . Learned solution (left panel); Numerical solution (right panel). NLS with potential $U(x)$ specified by (3.14) (top row), and a time-dependent potential $V(x, t)$ specified by (3.13) (bottom row).

Example 3.7 (The 2D cubic Schrödinger equation). We consider here the cubic Schrödinger equation (2.2) in 2D. The problem is set up as follows: We consider the solution of (2.2) in a compact domain $\Omega = [-\Omega_0\pi, \Omega_0\pi] \times [-\Omega_0\pi, \Omega_0\pi]$ with $\Omega_0 = 2$. The solutions in Ω are represented at grid points with $N_x = N_y = 64$. The solution in time up to $T = 1$ is represented at equally spaced time steps with $N_t = 100$. The training and testing are both handled within the domain Ω . For the parameters in the

wave packet, we choose $\mathcal{K} = \{1, 2, \dots, 5\}$ and we pick $(k_1, k_2) \in \mathcal{K} \times \mathcal{K}$ and $\Sigma = \{h, 2h, 3h, 4h, 5h, 6h\}$ with $h = 0.25$.

To generate a reference solution, we choose a larger domain $[-2\Omega_0\pi, 2\Omega_0\pi] \times [-2\Omega_0\pi, 2\Omega_0\pi]$ so that it represents solutions over the entire space within the time period under consideration. For the network, we choose an FCNN with $D = 4$, $m_1 = N_x N_y$, $m_2 = N_x N_y$ and $M = 100$. The network is trained for 40000 epochs. Then we use the network to predict the solution of the 2D cubic Schrödinger equation (2.2) with initial condition:

$$(3.15) \quad u_0(x_1, x_2) = \exp[-(x_1^2 + x_2^2) + i(3x_1 + 3x_2)].$$

The results are presented in Figure 9. The corresponding relative errors for the density, the real and imaginary parts of the wave function are 7.91×10^{-3} , 8.98×10^{-3} , and 8.14×10^{-3} , respectively. The results will improve if we choose $\mathcal{K} = \{1, 2, \dots, 5\}$ but $\Sigma = \{h, 1.1h, 1.2h, 1.3h, 1.4h, 1.5h\}$ with $h = 0.8$ which give the relative error 6.48×10^{-3} , 6.53×10^{-3} and 5.73×10^{-3} for the density, the real part, and the imaginary parts, respectively. Notice that at time $T = 1$, part of the wave packets have moved out of Ω . Therefore, the network has shown an “absorbing” property.

Example 3.8 (Wave propagation in irregular domains). We extend the previous example to irregular domains. Specifically, we consider a circular disk, and an L-shape domain. This does not impose further difficulty on the method: We simply repeat the training procedure over the corresponding domains. As shown in Figure 10 for the disk domain, the corresponding relative errors for the density, the real and imaginary parts of the wave function are 1.21×10^{-2} , 9.99×10^{-3} , 8.28×10^{-3} for $\mathcal{K} = \{1, 2, 3, 4, 5\}$, $\Sigma = \{h, 2h, 3h, 4h, 5h, 6h\}$ with $h = 0.25$ and 4.88×10^{-3} , 8.08×10^{-3} , 8.01×10^{-3} for $\Sigma = \{h, 1.1h, 1.2h, 1.3h, 1.4h, 1.5h\}$ with $h = 0.8$, respectively. As shown in Figure 11 for the L-shape domain, the corresponding relative errors for the density, the real and imaginary parts of the wave function are 7.86×10^{-3} , 9.45×10^{-3} , 8.77×10^{-3} for $\mathcal{K} = \{1, 2, 3, 4, 5\}$, $\Sigma = \{h, 2h, 3h, 4h, 5h, 6h\}$ with $h = 0.25$ and 9.46×10^{-3} , 1.18×10^{-2} , 8.94×10^{-3} for $\Sigma = \{h, 1.1h, 1.2h, 1.3h, 1.4h, 1.5h\}$ with $h = 0.8$, respectively. In both cases, the neural network has demonstrated an absorbing property, allowing the waves to propagate out of a domain with complex geometry.

4. DISCUSSION AND CONCLUSIONS

In this paper, we have proposed a machine-learning method to solve wave equations over unbounded domains without introducing artificial boundary conditions. As examples, we considered the Schrödinger equation and the second-order acoustic wave equation. Results show that the proposed method has good interpolative accuracy and some extrapolative accuracy.

All simulations are implemented in MacBook Pro Intel Core i5 (1 CPU, 4 Kernels and 8 Gb random access memory). The method provides an alternative for finite-time simulation of wave propagation. On the other hand, we found that wave propagations over long time period still remains a challenge for the neural network approximation.

Unlike conventional numerical methods for solving wave equations, e.g., [4, 15], results for rigorous error bounds from neural network approximations of PDEs over unbounded domains are scarce. Therefore we rely on extensive numerical experiments and we report some direct observations here.

Neural network as a PDE solver. Recently, the machine learning approach has been applied to wave equations in [11]. It is important to point out though that most of those effort focused on solving PDEs using neural networks on *bounded* domains [35, 37, 40, 47], while the current work is aimed at representing solutions of time-dependent hyperbolic PDEs on unbounded domains.

The choice of the data set and network structures. It is apparent from the numerical tests that the accuracy of the neural network representation depends crucially on the choice of the training set, as well as the network structure and the activation functions. When the test set lies in the training sets (or the range), we interpret the representation (2.8) as an interpolation. The accuracy is generally satisfactory with the error on the scale of 10^{-3} . We observe that the tanh function for the second-order

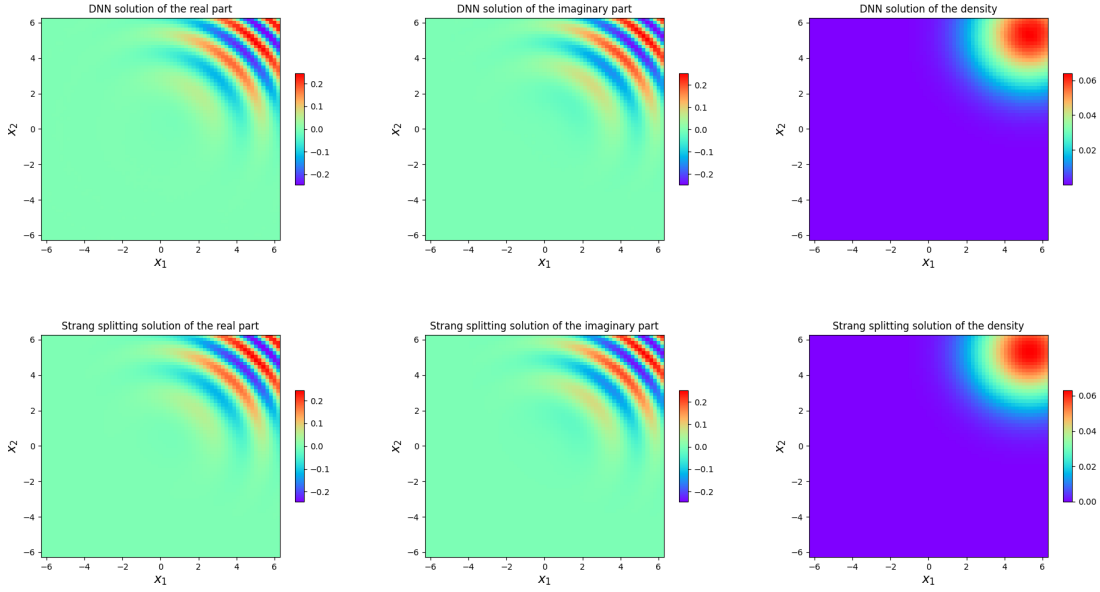


FIGURE 9. Solution of the 2D cubic Schrödinger equation in a square domain by the DNN (Top row), direct numerical method (Bottom row), evaluated at time $T = 1$ for the initial condition (3.15). A network with activation function \tanh is trained for 40000 iterations to represent the solutions. Left panel: the real part of wave packet solution; Middle panel: the imaginary part; Right panel: the electron density ρ .

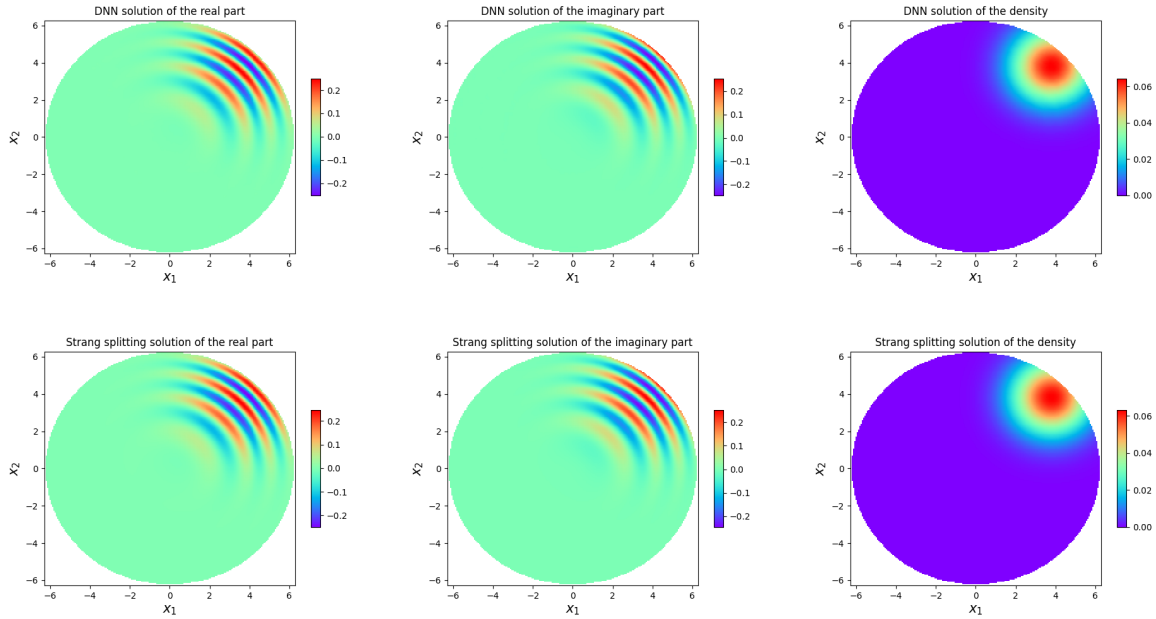


FIGURE 10. Solution of the 2D cubic Schrödinger equation in a circular domain by the DNN (Top row), direct numerical method (Bottom row), evaluated at time $T = 1$ for the initial condition (3.15). Here the activation function \tanh is used and the training takes 40000 iterations. Left panel: the real part of wave packet solution; Middle panel: the imaginary part; Right panel: the electron density ρ .

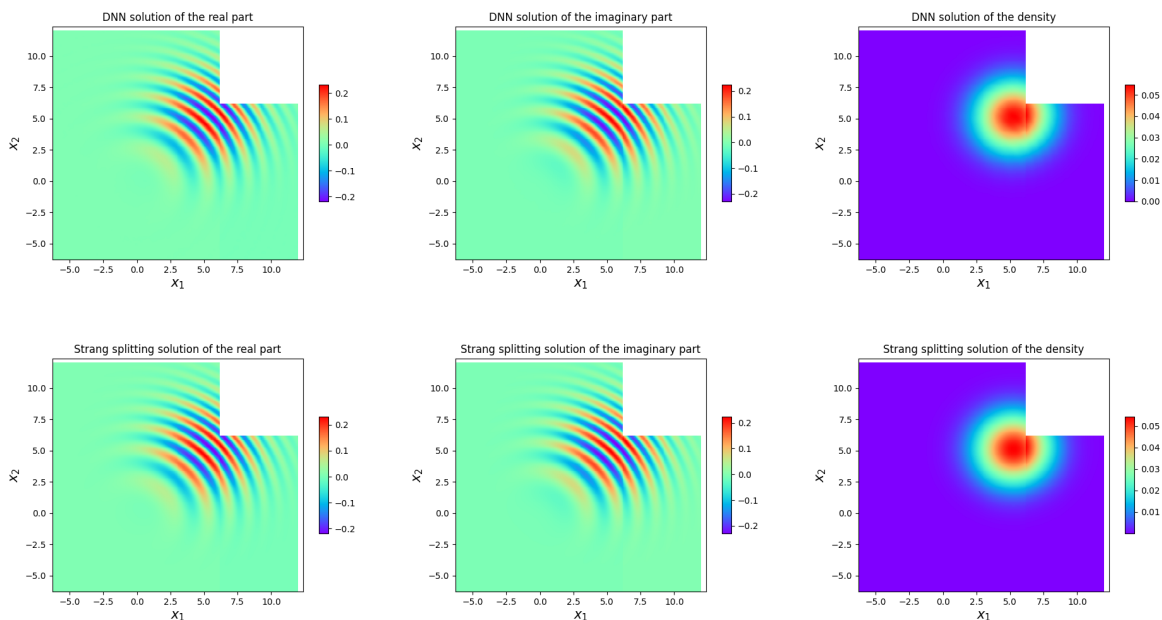


FIGURE 11. Solution of the 2D cubic Schrödinger equation in an L-shape domain by the DNN (Top row), direct numerical method (Bottom row), evaluated at time $T = 1$ for the initial condition (3.15). Here the activation function \tanh is used and the network is trained for 40000 iterations. Left panel: the real part of wave packet solution; Middle panel: the imaginary part; Right panel: the electron density ρ .

acoustic wave equation stood out as the best choice with robust overall performance in both FCNN and ResNet, as suggested by the comparison in Table 2, while the relu function for the Schrödinger equation is the best choice in Table 4. The comparison between the performance of FCNN and ResNet seems more subtle; The ResNet seems to perform better in more cases.

In contrast to interpolations, extrapolations can arise in different ways. For instance, the initial condition can be of a different function form than those in the training set. Results in Figure 6 are such examples. FCNNs seem to offer consistent results in this case. An extrapolation also comes up when the network (2.8) is used to predict solutions at a later time. We observed from Table 6 that the accuracy of such an approximation can be guaranteed for a short time period, and the FCNN with elu activation function yields much better results than other choices. Another scenario of an extrapolation is when the wave number (or the width of the packet) in the initial condition is outside the range of the set \mathcal{K} (or Σ) that is associated with the training set. Generally, the error grows when the wave number is further away from the set \mathcal{K} . But for a specific case, the results among different choices of the activation functions are mixed. The activation function elu seems to give reasonable accuracy in all the cases tested.

Due to the wave propagation nature, we proposed to use wave packets to create the training set. So far, our numerical tests have not singled out an optimal strategy. Although larger selections of \mathcal{K} and Σ generally give better results, they inevitably lead to larger training dataset. One possible direction is to start with a larger set of training data, and then use the proper orthogonal decomposition (POD) to extract the most relevant basis. In high dimensions, we might use the (quasi-) Monte Carlo methods to handle and extract the representative elements of Σ and \mathcal{K} .

The current approach excludes nonlinear waves, e.g., shock waves [14], contact discontinuities, solitons [23], etc. It would be interesting to investigate the performance of the neural network in those scenarios as well.

The relation to absorbing boundary conditions. The current approach targets the same type of problems as absorbing boundary conditions, viz., wave propagation processes that occur in an unbounded domain, but are triggered by initial conditions or external signals that are localized in a bounded domain. However, rather than using the neural network to incorporate the absorbing boundary condition into the FDTD procedure [12, 48, 53, 54], which involves the history of solutions at the boundary, we directly map the initial condition to the solution at time instances of interest. The numerical results suggest that such an approximation also exhibits absorbing properties. In addition to the wave equations we discussed in this paper, the results suggest that this framework can be extended to other wave propagation problems, e.g., those from fluid mechanics [26], elasticity [6, 25], and molecular dynamics [18, 34, 39].

High-dimensional problems. One of the distinct advantage of neural networks is the ability to treat high-dimensional problems. This has been demonstrated in various type of PDEs. A potential application of the current approach is to many-particle Schrödinger equations. For instance, in ionization problems, electrons can be driven away from nuclei via a laser field, and traditionally, such problems have been treated using effective models and absorbing boundary conditions, e.g., in the context of time-dependent density-functional theory [51]. This work is currently underway.

ACKNOWLEDGMENTS

This work is supported in part by the financial support from the program of China Scholarships Council No. 201906920043 (C. Xie), National Science Foundation of China Grant No. 11971021 (J. Chen).

REFERENCES

- [1] X. Antoine, A. Arnold, C. Besse, M. Ehrhardt, and A. Schädle, *A review of artificial boundary conditions for the Schrödinger equation*, PAMM: Proc. Appl. Math. Mech., 2007, pp. 1023201–1023202.
- [2] X. Antoine, W. Bao, and C. Besse, *Computational methods for the dynamics of the nonlinear Schrödinger/Gross–Pitaevskii equations*, Comput. Phys. Commun. **184** (2013), no. 12, 2621–2633.
- [3] A. Arnold, M. Ehrhardt, and I. Sofronov, *Discrete transparent boundary conditions for the Schrödinger equation: Fast calculation, approximation, and stability*, Commun. Math. Sci. **1** (2013), no. 3, 501–556.
- [4] G. Bao and H. Wu, *Convergence analysis of the perfectly matched layer problems for time-harmonic Maxwell’s equations*, SIAM J. Numer. Anal. **43** (2005), no. 5, 2121–2143.
- [5] W. Bao, S. Jin, and P.A. Markowich, *On time-splitting spectral approximations for the Schrödinger equation in the semiclassical regime*, J. Comput. Phys. **175** (2002), no. 2, 487–524.
- [6] E. Becache, P. Joly, and C. Tsogka, *Fictitious domains, mixed finite elements and perfectly matched layers for 2-D elastic wave propagation*, J. Comput. Acous. **9** (2001), no. 03, 1175–1201.
- [7] C. Beck, W. E, and A. Jentzen, *Machine learning approximation algorithms for high-dimensional fully nonlinear partial differential equations and second-order backward stochastic differential equations*, J. Nonlinear Sci. **29** (2019), no. 4, 1563–1619.
- [8] S. Becker, R. Braunwarth, M. Hutzenthaler, A. Jentzen, and P. Wurstemberger, *Numerical simulations for full history recursive multilevel Picard approximations for systems of high-dimensional partial differential equations*, Commun. Comput. Phys. **28** (2020), 2109–2138.
- [9] J.P. Berenger, *A perfectly matched layer for the absorption of electromagnetic waves*, J. Comput. Phys. **114** (1994), no. 2, 185–200.
- [10] L. Bottou, F. Curtis, and J. Nocedal, *Optimization methods for large-scale machine learning*, SIAM Rev. **60** (2018), no. 2, 223–311.
- [11] W. Cai, X. Li, and L. Liu, *A phase shift deep neural network for high frequency approximation and wave problems*, SIAM J. Sci. Comput. **42** (2019), no. 5, A3285–A3312.
- [12] Y. Chen and N. Feng, *Learning Unsplit-field-based PML for the FDTD method by deep differentiable forest*, arXiv:2004.04815 (2020).
- [13] Y. Chen, L. Lu, G. Karniadakis, and L. Negro, *Physics-informed neural networks for inverse problems in nano-optics and metamaterials*, Opt. Express **28** (2020Apr), no. 8, 11618–11633.
- [14] C.M. Dafermos, *Hyperbolic conservation laws in continuum physics*, Vol. 3, Springer, 2005.
- [15] J. Diaz and P. Joly, *A time domain analysis of PML models in acoustics*, Comput. Methods Appl. Mech. Eng. **195** (2006), no. 29–32, 3820–3853.

- [16] W. E, *Machine learning and computational mathematics*, Commun. Comput. Phys. **28** (2020), no. 5, 1639–1670.
- [17] W. E, J. Han, and A. Jentzen, *Deep learning-based numerical methods for high-dimensional parabolic partial differential equations and backward stochastic differential equations*, Commun. Math. Statist. **5** (2017), no. 4, 349–380.
- [18] W. E and Z. Huang, *Matching conditions in atomistic-continuum modeling of materials*, Phys. Rev. Lett. **87** (2001), no. 13, 135501.
- [19] W. E and B. Yu, *The deep Ritz method: a deep learning-based numerical algorithm for solving variational problems*, Commun. Math. Statist. **6** (2018), no. 1, 1–12.
- [20] B. Engquist and A. Majda, *Absorbing boundary conditions for numerical simulation of waves*, Proceed. National Acad. Sci. **74** (1977), no. 5, 1765–1766.
- [21] A.C. Eringen and G.A. Maugin, *Electrodynamics of continua i: foundations and solid media*, Springer-Verlag New York, 1990.
- [22] L.C. Evans, *Partial differential equations*, 2nd ed., American Mathematical Society, 2010.
- [23] M.G. Forest and J.E. Lee, *Geometry and modulation theory for the periodic nonlinear Schrödinger equation*, 1986, pp. 35–69.
- [24] D. Givoli, *Computational absorbing boundaries*, In: Marburg S., Nolte B. (eds) Computational acoustics of noise propagation in fluids-finite and boundary element methods, 2008, pp. 145–166.
- [25] M.N. Guddati and J.L. Tassoulas, *Continued-fraction absorbing boundary conditions for the wave equation*, J. Comput. Acous. **8** (2000), no. 01, 139–156.
- [26] H. Han and W. Bao, *An artificial boundary condition for two-dimensional incompressible viscous flows using the method of lines*, Inter. J. Numer. Methods Fluids **22** (1996), no. 6, 483–493.
- [27] H. Han and X. Wu, *Artificial boundary method*, Springer Science and Business Media, 2013.
- [28] J. Han, A. Jentzen, and W. E, *Solving high-dimensional partial differential equations using deep learning*, Proceed. National Acad. Sci. **115** (2018), no. 34, 8505–8510.
- [29] K. He, X. Zhang, S. Ren, and J. Sun, *Deep residual learning for image recognition*, CoRR **1512.03385** (2015).
- [30] ———, *Delving deep into rectifiers: Surpassing human-level performance on ImageNet classification*, Proc. IEEE Inter. Conf. Computer Vision, 2015, pp. 1026–1034.
- [31] M. Hutzenthaler, A. Jentzen, and P. Wurstemberger, *Overcoming the curse of dimensionality in the approximative pricing of financial derivatives with default risks*, Electron. J. Probab. **25** (2020), no. 101, 73.
- [32] S. Jiang and L. Greengard, *Fast evaluation of nonreflecting boundary conditions for the Schrödinger equation in one dimension*, Comput. Math. Appl. **47** (2004), no. 6-7, 955–966.
- [33] X. Jin, S. Cai, H. Li, and G. Karniadakis, *NSFnets (Navier-Stokes flow nets): Physics-informed neural networks for the incompressible Navier-Stokes equations*, J. Comput. Phys. (2020), 109951.
- [34] E.G. Karpov, G.J. Wagner, and W.K. Liu, *A Green's function approach to deriving non-reflecting boundary conditions in molecular dynamics simulations*, Inter. J. Numer. Methods Eng. **62** (2005), no. 9, 1250–1262.
- [35] Y. Khoo, J. Lu, and L. Ying, *Solving parametric PDE problems with artificial neural networks*, European J. Appl. Math. (2020).
- [36] D.P. Kingma and J. Ba, *Adam: A method for stochastic optimization*, CoRR (2015).
- [37] I. Lagaris, A. Likas, and D. Fotiadis, *Artificial neural networks for solving ordinary and partial differential equations*, IEEE Trans. Neur. Netw. **9** (1998), no. 5, 987–1000.
- [38] B. Li, J. Zhang, and C. Zheng, *An efficient Second-Order finite difference method for the One-Dimensional Schrödinger equation with absorbing boundary conditions*, SIAM J. Numer. Anal. **56** (2018), no. 2, 766–791.
- [39] X. Li and W. E, *Variational boundary conditions for molecular dynamics simulations of solids at low temperature*, Commun. Comput. Phys. **1** (2006), no. 1, 135–175.
- [40] L. Lyu, Z. Zhang, M. Chen, and J. Chen, *MIM: A deep mixed residual method for solving high-order partial differential equations*, arXiv:2006.04146 (2020).
- [41] F. Moxley, D. Chuss, and W. Dai, *A generalized finite-difference time-domain scheme for solving nonlinear Schrödinger equations*, Comput. Phys. Commun. **184** (2013), no. 8, 1834–1841.
- [42] J. Nocedal and S.J. Wright, *Numerical optimization*, Springer, New York, NY, 1999.
- [43] M. Raissi, P. Perdikaris, and G. Karniadakis, *Physics-informed neural networks: A deep learning framework for solving forward and inverse problems involving nonlinear partial differential equations*, J. Comput. Phys. **378** (2019), 686–707.
- [44] M. Raissi, A. Yazdani, and G. Karniadakis, *Hidden fluid mechanics: Learning velocity and pressure fields from flow visualizations*, Science **367** (2020), 1026–1030.
- [45] H. Robbins and S. Monro, *A stochastic approximation method*, Ann. Math. Statist. **22** (1951), 400–407.
- [46] T. Shibata, *Absorbing boundary conditions for the finite-difference time-domain calculation of the one-dimensional Schrödinger equation*, Phys. Rev. B **43** (1991), no. 8, 6760.
- [47] J. Sirignano and K. Spiliopoulos, *DGM: A deep learning algorithm for solving partial differential equations*, J. Comput. Phys. **375** (2018), 1339–1364.

- [48] F. Wang, Z. Yang, and C. Yuan, *Practical absorbing boundary conditions for wave propagation on arbitrary domain*, Adv. Appl. Math. Mech. **12** (2020), no. 6, 1384–1415.
- [49] G.B. Whitham, *Linear and nonlinear waves*, Vol. 42, John Wiley and Sons, 2011.
- [50] X. Wu and X. Li, *Absorbing boundary conditions for the time-dependent Schrödinger-type equations in \mathbb{R}^3* , Phys. Rev. E **101** (2020), no. 1, 013304.
- [51] K. Yabana, T. Nakatsukasa, J.I. Iwata, and G.F. Bertsch, *Real-time, real-space implementation of the linear response time-dependent density-functional theory*, Physica Status Solidi (B) Basic Research **243** (2006apr), no. 5, 1121–1138 (en).
- [52] L. Yang, X. Meng, and G. Karniadakis, *B-PINNs: Bayesian physics-informed neural networks for forward and inverse PDE problems with noisy data*, J. Comput. Phys. **425** (2021), 109913.
- [53] H. Yao and L. Jiang, *Machine-learning-based PML for the FDTD method*, IEEE Ante. Wire. Prop. Lett. **18** (2018), no. 1, 192–196.
- [54] ———, *Enhanced PML based on the long short term memory network for the FDTD method*, IEEE Access **8** (2020), 21028–21035.
- [55] A. Yazdani, L. Lu, M. Raissi, and G. Karniadakis, *Systems biology informed deep learning for inferring parameters and hidden dynamics*, PLoS Comput. Bio. **16** (2020), no. 11, e1007575.
- [56] H. Yoshida, *Construction of higher order symplectic integrators*, Phys. Lett. A **150** (1990), no. 5-7, 262–268.
- [57] Y. Zang, G. Bao, X. Ye, and H. Zhou, *Weak adversarial networks for high-dimensional partial differential equations*, J. Comput. Phys. **411** (2020), 109409.

SCHOOL OF MATHEMATICAL SCIENCES, SOOCHOW UNIVERSITY, SUZHOU, CHINA.
Email address: 20184007005@stu.suda.edu.cn

SCHOOL OF MATHEMATICAL SCIENCES, SOOCHOW UNIVERSITY, SUZHOU, CHINA.
Email address: jingrunchen@suda.edu.cn (Corresponding author)

DEPARTMENT OF MATHEMATICS, THE PENNSYLVANIA STATE UNIVERSITY, UNIVERSITY PARK, PA 16802, USA.
Email address: xiantao.li@psu.edu (Corresponding author)